Coherence effects in nuclear bremsstrahlung

Lohner, H; TAPS Collaboration

COHERENCE EFFECTS IN NUCLEAR BREMSSTRAHLUNG*

H. Löhner

KVI Groningen, Zernikelaan 25, 9747 AA Groningen, The Netherlands

and the TAPS Collaboration:

KVI Groningen, The Netherlands
GANIL Caen, France
IFIC Valencia, Spain
GSI Darmstadt, Germany
University Giessen, Germany
NPI Řež u Prahy, Czech Republic

The production of nuclear bremsstrahlung ($E_\gamma > 30\,\text{MeV}$) has been studied in heavy-ion collisions, as well as proton and α-particle collisions with nuclei. In heavy-ion reactions the measured photon spectra show an exponential shape dominated by the incoherent sum of photons produced in first-chance collisions. Photon spectra, angular distributions and multiplicities at $60A$ MeV indicate that a significant fraction of photons is emitted in secondary nucleon–nucleon collisions from a thermally equilibrated system. In 200 MeV $\alpha + p$ collisions the incoherent contribution to the photon spectrum is observed as well at low photon energies, while coherent bremsstrahlung is observed at the highest photon energies from radiative capture into unbound states of ^{5}Li. In 190 MeV proton reactions with light and heavy targets photon spectra have been measured up to the kinematic limit. At high photon energies the spectra show the expected behaviour from first-chance collisions. Below ca 80 MeV a significant suppression of the photon yield is observed. We attribute this effect to the interference of photon amplitudes due to multiple scattering of nucleons in the nuclear medium.

PACS numbers: 13.40.–f, 13.75.–n, 13.75.Cs, 25.10.+s

1. Introduction

In collisions between nucleons electromagnetic radiation can be emitted due to the rapid change in the nucleon velocity (bremsstrahlung). Accordingly, in nucleus–nucleus collisions bremsstrahlung is emitted due to the individual collisions of the constituent nucleons. Despite their low production rates, photons are a unique probe of the dynamical evolution of the nuclear system created in nucleus–nucleus or proton–nucleus collisions. At variance with charged particles and nuclear fragments, photons are primordial observables because they do not suffer final-state interactions from Coulomb or strong interactions with the surrounding medium, thus providing an undisturbed image of the photon production process. Earlier experiments with protons and heavy ions [1] indicated that bremsstrahlung is dominantly produced in first-chance proton–neutron collisions. Consequently, dynamical nuclear reaction models include photon production in the incoherent quasi-free collision limit, *i.e.*, free nucleon–nucleon (NN) bremsstrahlung cross sections are employed assuming on-shell nucleons and the intensities of the individual scattering processes are added rather than their amplitudes. Hard-photons have thus been exploited to probe the pre-equilibrium conditions prevailing in the initial high-density phase of nucleus–nucleus reactions [2,3].

At sufficiently high incident energies there is enough energy available for photon production in subsequent collisions. Therefore multiple-scattering processes become important in reactions of protons with nuclei. A significant effect on the radiation process is expected due to the influence of multiple scattering and off-shell propagation of nucleons. In this case, the bremsstrahlung amplitudes from different steps in the scattering process interfere and, therefore, the individual bremsstrahlung contributions may not be added incoherently. This so called LPM effect was predicted by Landau, Pomerančuk, and Migdal [4] for the successive Coulomb scattering of electrons in matter, resulting in a reduced bremsstrahlung rate once the mean free path is shorter than the coherence length. This suppression has been reported for pair creation from cosmic-ray photons [5], and for bremsstrahlung from high-energy electrons [6] in accelerator experiments. The general importance of coherence effects on particle production and absorption in (non)-equilibrium dense matter has been discussed in the literature [7–9]. Such effects are, *e.g.*, relevant for soft photon and dilepton production in hot hadronic matter [10, 11]. However, no quantitative analysis for the LPM effect in nuclear bremsstrahlung has been reported so far. To study the influence of the nuclear medium on the bremsstrahlung spectrum we have measured the energy spectra and angular distributions of photons up to the

kinematic limit in reactions of 190 MeV protons with a range of targets. A strong suppression of bremsstrahlung relative to a quasi-free production model is observed in the low-energy regime of the photon spectrum, contrary to observations in heavy-ion collisions.

2. Experiment

Here we report on some aspects of the experimental program with the photon spectrometer TAPS [12,13] at the AGOR facility of the KVI Groningen using ^{36}Ar, α and proton beams. The photon spectrometer TAPS was configured in 6 blocks of 64 BaF$_2$ crystals each at a distance of 66 cm from the target. The setup covered the polar angular range between 57° and 176° on both sides of the beam with an azimuthal acceptance of $-21° < \phi < 21°$. The granularity of the TAPS setup resulted in an angular resolution of 5.2°. Photons were separated from nuclear particles via their time-of-flight with respect to the Radio-Frequency signal (RF) of the cyclotron. The time resolution was about 1 ns (FWHM). In addition, pulse-shape discrimination was employed. The event trigger required an energy deposition of at least 5 MeV in a BaF$_2$ module. The signals from the plastic veto detectors in front of the BaF$_2$ scintillators were used to select photons and protons on the trigger level. The relative energy calibration was determined from the characteristic energy deposited by cosmic-ray muons. The absolute calibration was provided by the π^0 mass peak and the 15.1 MeV photons originating from inelastic proton scattering on ^{12}C. A small residual background from cosmic-ray muons within the trigger gate was removed by subtracting the photon spectrum obtained by gating on a random time window with respect to the RF.

Two-photon invariant mass spectra from events with two coincident photons were analysed in order to obtain the π^0 decay contribution. The raw π^0 distributions were corrected for the finite acceptance and the response of TAPS. The measured pion distribution was extrapolated by Monte Carlo simulations [14,15] into regions of missing acceptance by analysing the angular distributions in small energy bins of 2 MeV.

In the heavy-ion experiments two phoswich multi-detectors, the Washington University "Dwarf Ball" (DB) [16] and the KVI "Forward Wall" (FW) [17], were added to TAPS to allow the isotopic identification of the Light Charged Particles (LCP: p, d, t, ^{3}He and α) and the charge of the intermediate mass fragments up to that of the projectile by means of pulse-shape techniques. The DB was composed of 64 BC400–CsI(Tl) phoswich telescopes in the angular range $32° < \theta < 168°$, and the FW hodoscope comprised 92 NE102A–NE115 ΔE–E phoswich detectors in the forward region $(2.5° < \theta < 25°)$.

3. Thermal photons

The inclusive and exclusive hard-photon and fragment production in ^{36}Ar+^{197}Au at $60A$ MeV, and the inclusive hard-photon production in the ^{36}Ar+^{107}Ag, ^{58}Ni, ^{12}C reactions at $60A$ MeV have been studied. The hard-photon spectra of the Au, Ag and Ni targets feature two distinct components above 30 MeV (Fig. 1 left, for the Au target). These spectra can be described by the sum of two exponential distributions characterized by inverse slopes E_0^d and E_0^t, corresponding to a "direct" (first-chance) and a "thermal" component originating from secondary $pn\gamma$ processes [18]. The direct slopes of the three heaviest targets, $E_0^d \approx 20$ MeV, are two to three times larger than the thermal ones, $E_0^t \approx 6$–9 MeV, and the thermal contribution represents 15%–20% of the total yield.

Such thermal hard-photons hence constitute a novel and clean probe of the intermediate dissipative stages of the reaction where nuclear fragmentation can take place. Photons thus may provide the time-scale of such reactions and allow to characterise the thermodynamical state of the fragmenting source. The observation of thermal hard-photons in coincidence
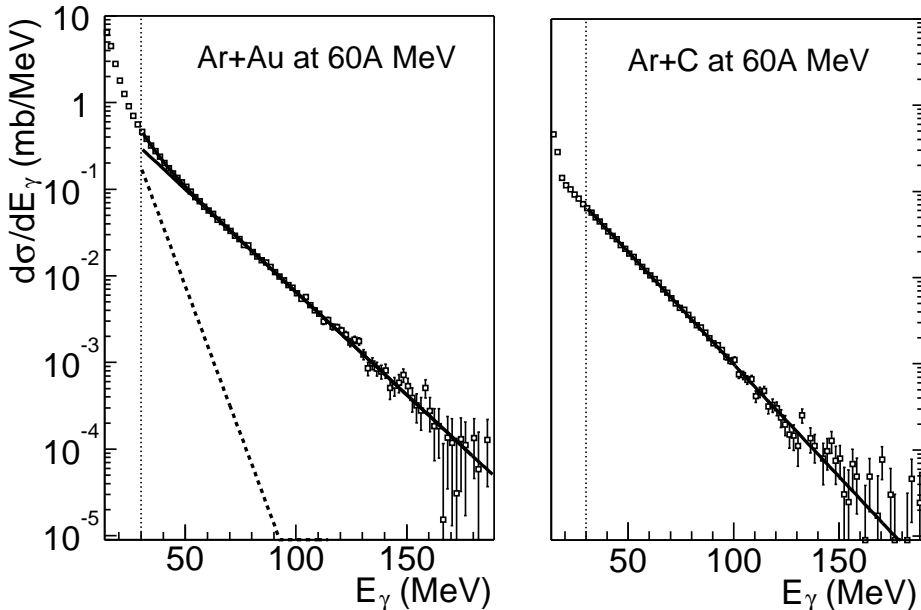

Fig. 1. Photon spectra ($E_\gamma > 30$ MeV) for $60A$ MeV ^{36}Ar collisions. Left: ^{36}Ar+Au spectrum fitted by the sum of two exponential distributions, a direct (solid line) and a thermal (dashed line) contribution; right: ^{36}Ar+C spectrum fitted by a single exponential distribution.

with intermediate-mass fragment emission in the ^{36}Ar+^{197}Au system indicates that multifragmentation is, at least for this reaction, a slow process preceded by the thermalization of the system.

No thermal component is apparent in the photon spectrum measured in the ^{36}Ar+^{12}C reaction and direct bremsstrahlung alone accounts for the whole photon emission already above $E_\gamma \approx 20$ MeV (Fig. 1, right). Such a light system does not provide a sufficient number of nucleon–nucleon collisions needed for thermalization to take place. Thus, pure first-chance bremsstrahlung dominates the entire bremsstrahlung emission.

4. Coherent bremsstrahlung

From hard photon production in heavy-ion reactions the generally accepted picture emerged that the incoherent superposition of bremsstrahlung processes in individual NN collisions is the dominating process. For the first time coherent bremsstrahlung could be demonstrated in the $\alpha + p$ system studied at $50A$ MeV [19]. Because of the strong binding of the α-particle, the quasi free process can only lead to bremsstrahlung with $E_\gamma < 22$ MeV, while at higher energy, up to the kinematic limit of $E_{max} = 39$ MeV, bremsstrahlung can only be produced coherently in this reaction. In fact, we find coherently produced hard photons to be the dominant radiative process in the $\alpha + p$ system. After transformation to the $\alpha + p$ center-of-mass

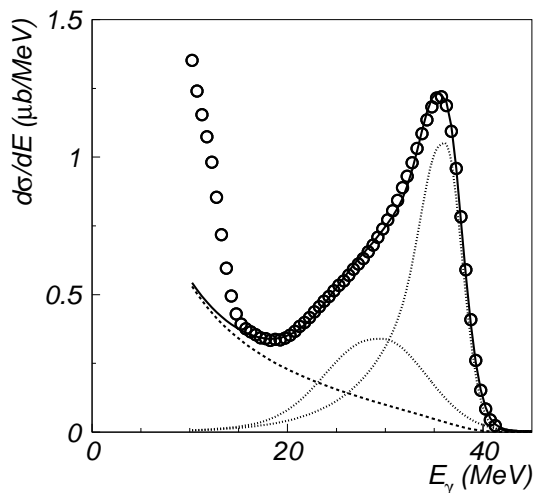Fig. 2. Inclusive photon energy spectrum (in the c.m. frame) for the $\alpha + p$ reaction at 50 MeV/nucleon. The statistical errors are smaller than the symbols. The global fit (solid line) is decomposed into the classical bremsstrahlung spectrum (dashed line) and two contributions representing capture to the two low-lying resonances in ^{5}Li, *i.e.* the unbound ground state and the first excited state (dotted lines).

frame the photon energy spectra at all angles exhibit the same characteristic shape as shown in Fig. 2. The shape of this spectrum is very different from that of the hard photons in nucleus–nucleus reactions. The low-energy photon spectrum appears to have a classical $1/E_\gamma$ shape. Photons with energies close to the kinematic limit have been associated with direct capture to the two lowest states of the unbound ^{5}Li. The data have been compared with model calculations in which coherent bremsstrahlung and direct capture are treated consistently as one and the same process. The calculations qualitatively reproduce these two features of the data.

The studies of coherent bremsstrahlung from the direct capture to the lowest states of the unbound ^{5}Li have motivated the extension of this technique to study ^{6}He. In particular, the configuration of the two halo neutrons relative to the α core might lead to different capture processes on various subsystems of ^{6}He. Direct capture on the constituents of ^{6}He might be observed as a quasi-free process in addition to capture into ^{7}Li. The experiment was carried out at GANIL with a $40A$ MeV ^{6}He beam on a proton target [20].

The Quasi-Free Capture (QFC) processes were investigated by measuring photons in coincidence with fragments lighter than ^{7}Li. Photon energy spectra and fragment momentum distributions are compared in Fig. 3 with a QFC model. Inclusion of the fragment final-state interaction appears important to correctly describe the measured fragment momentum distributions. Fig. 3(c),(d) reveals evidence for QFC on the α core, whereby the two halo neutrons behave as spectators. The photon spectrum measured in coincidence with α particles resembles that observed for the $\alpha + p$ reaction shown in Fig. 2. The background, however, arising from ^{6}He breakup, in which the α particle is detected and the halo neutrons interact with the photon detector, is significant (dotted line in Fig. 3(c)). Therefore, also α–γ-n coincidences have been studied, for which some 30 events were observed. The resulting spectra exhibit the $1/E$ shape for neutrons (open squares) and, more importantly, a higher peak-to-continuum signal at 27 MeV for the photons (open circles) which is closer to that measured previously for the $p(\alpha, \gamma)^5$Li reaction.

In the case of ^{6}Li–γ coincidences, two lines were observed (Fig. 3(a)) at 30 and 3.5 MeV. These are clearly associated with the formation of ^{6}Li and the decay of the second excited state, at 3.56 MeV, the $T = 1$ analogue of ^{6}He g.s. Finally, d–γ coincidences present a peak in the photon energy spectrum at $E_\gamma = 20$–22 MeV (Fig. 3(e)). However, the QFC process on the two halo neutrons was not observed despite sufficient efficiency of the detection system. This suggests that the dominant configuration for the ^{6}He g.s. is ^{4}He–n–n with a relatively large n–n separation, in agreement with Ref. [21].
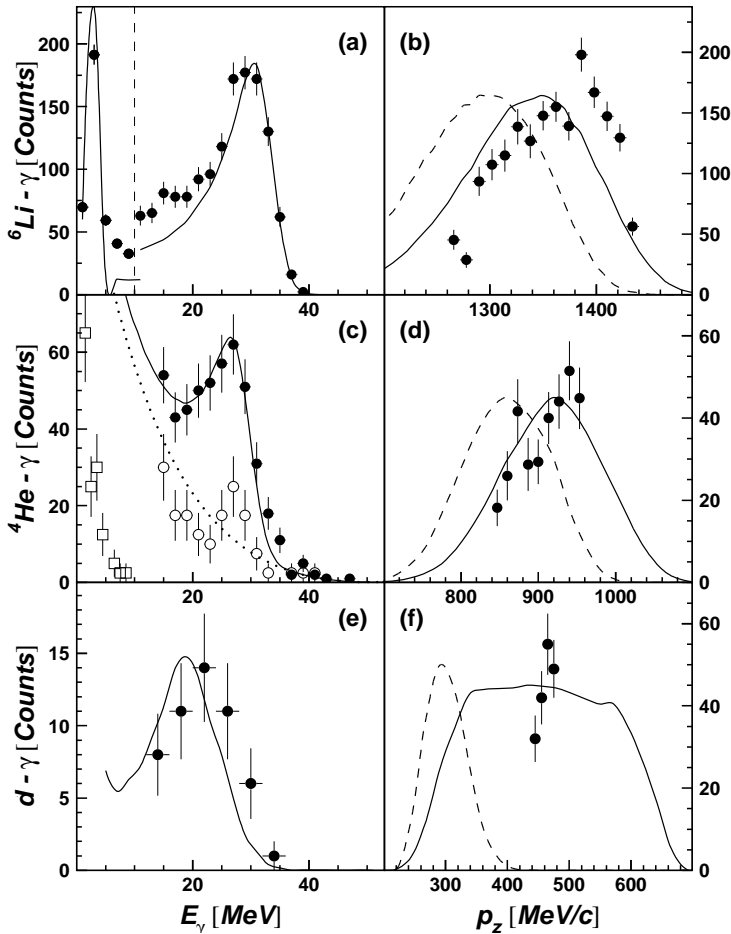
Fig. 3. Photon energy in the ^{6}He $+ p$ c.m. system (left) and momentum distribution of the coincident fragment (right) for ^{6}Li (upper), α particles (middle), and deuterons (lower panels). The solid lines are QFC calculations for the subclusters ^{5}He, α, and one halo neutron, respectively. The dashed lines on the right are without fragment FSI.

5. Soft bremsstrahlung suppression

To study the influence of the nuclear medium on the bremsstrahlung spectrum we have measured the energy spectra and angular distributions of photons up to the kinematic limit in reactions of 190 MeV protons with a range of targets. A strong suppression of bremsstrahlung relative to a quasi-free production model is observed in the low-energy regime of the

photon spectrum [22].   Fig. 4 shows a compilation of the photon spectra at a laboratory angle of 75° for the four targets studied here. The double differential cross sections have been normalized to the geometrical cross section $\sigma_r = 1.44\pi A^{2/3}$ fm^2 of each reaction with target mass number A. The spectra extend up to the kinematic limit $E_{\max}=T_{\mathrm{c.m.}} + Q$, where Q is the Q-value of the reaction and $T_{\mathrm{c.m.}}$ the center-of-mass energy. If plotted as function of the scaled photon energy $E_\gamma/E_{\max}$, all data in Fig. 4 above 100 MeV fall on the same curve [14,23] (Fig. 5). The shape of the photon spectra displays a plateau between 30 and 80 MeV and an exponential decrease towards the kinematic limit. This shape is different from photon spectra in heavy ion reactions [24,25], where nearly exponential slopes have been observed above 30 MeV. The rise at photon energies below 30 MeV for the heavier targets can be attributed to statistical photon emission.

For comparison with dynamical model calculations including the multiple-scattering process we employ the Intra-Nuclear Cascade (INC) code of Cugnon [26]. The INC model was chosen because it reproduces well many aspects of proton–nucleus reactions at these bombarding energies [27]. Furthermore it allows the study of photon–nucleon correlations [28] because it conserves

Fig. 4. Target-mass dependence of photon spectra for the C (circles), Ni (triangles), Ag (squares), and Au (crosses) targets at a laboratory angle of 75°. The double differential cross sections have been normalized to the geometrical reaction cross section.
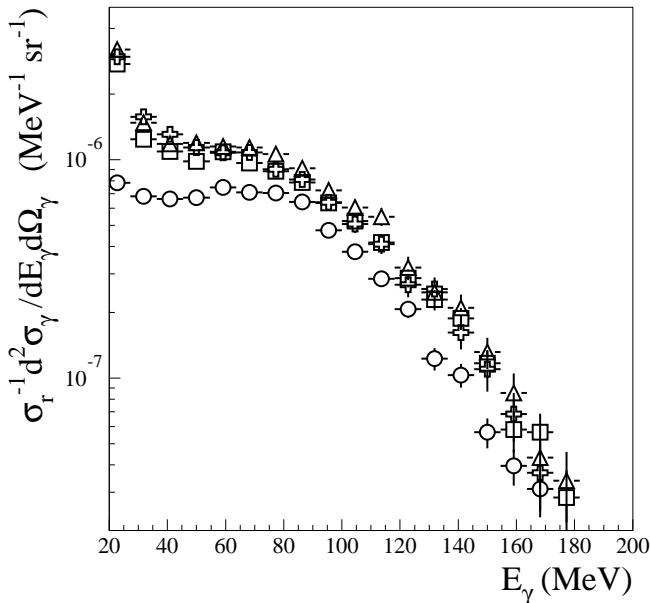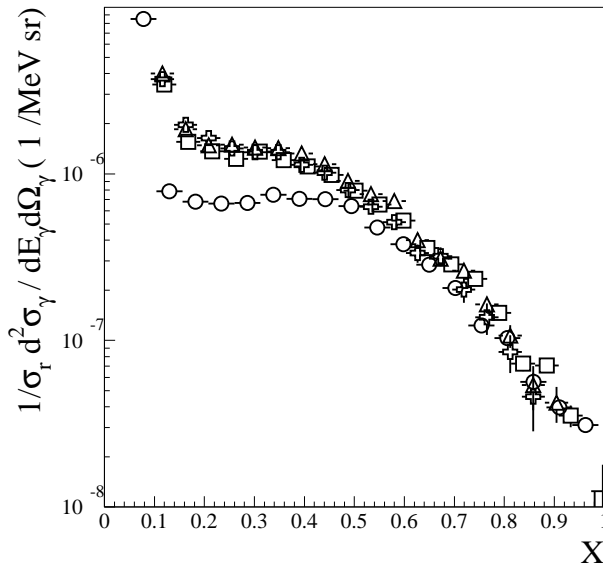
Fig. 5. Target-mass dependence of photon spectra for the C (circles), Ni (triangles), Ag (squares), and Au (crosses) targets at a laboratory angle of 75°. The double differential cross sections have been normalized to the geometrical reaction cross section and are plotted against the scaled photon energy $X = E_\gamma / E_{\max}$.

correlations between scattered particles. This is a necessary feature for the inclusion of the NN bremsstrahlung production in a non-perturbative manner with the kinematically correct $pn\gamma$ process using the Soft–Photon Approximation (SPA) for free pn bremsstrahlung [29]. We found that the optimal way to implement Pauli blocking in INC was achieved by requiring all final scattering states to lie above the Fermi surface. The nucleon phase-space distributions from the INC calculations agree well with those obtained using the Boltzmann–Uehling–Uhlenbeck (BUU) [30] transport model. The BUU results describe the photon spectrum ($E_\gamma > 30$ MeV) from $180A$ MeV Ar+Ca collisions fairly well [25] although slightly overpredicting the yield on the soft side of the spectrum.

Fig. 6 shows the photon spectrum for the Au target at 75° in comparison with the INC and BUU results. Both models agree quite well with each other in the full spectrum but overestimate significantly the experimental photon yield at low and intermediate photon energies ($E_\gamma \leq 100$ MeV). Good agreement between the experimental data and the calculations is found in the hard part of the spectrum, even near the kinematic limit. The multiple-
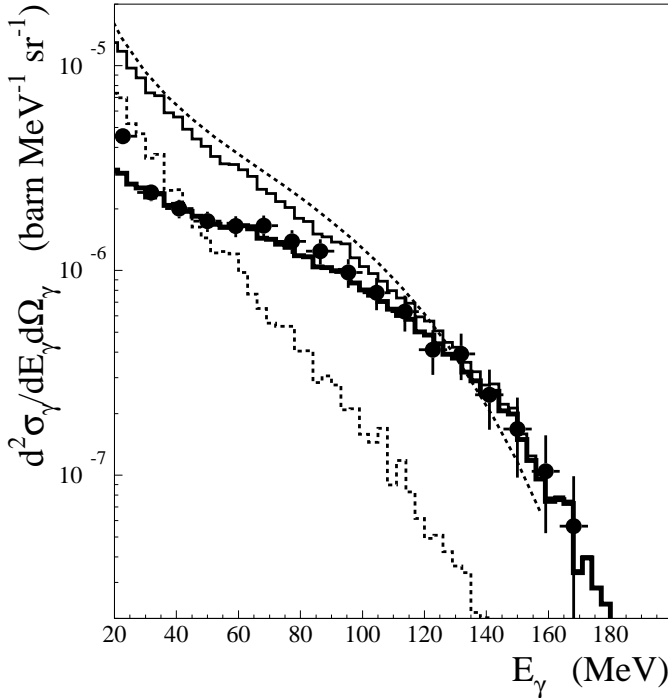
Fig. 6. Photon spectrum for 190 MeV p+Au at an angle of 75° (filled circles), compared to results of the INC (thin-line histogram) and BUU (dashed line) models. The dashed histogram shows the multiple-step contribution from the INC model. The thick-line histogram is the INC result multiplied with the quenching factor f_q from Eq. (1).

step contribution from INC has been indicated separately in Fig. 6. The overall agreement between experiment and theory would be much better if no multiple scattering was taken into account. It seems as if multiple-scattering processes are overestimated in theory. However, the amount of multiple scattering in INC has been checked against the experimental proton yields at large angles. These proton yields, in which multiple-scattering processes are essential, agree within the error margins for all targets studied [14]. Therefore, multiple scattering is well described.

In the nuclear medium the nucleon mean free path is $\lambda_{\mathrm{mfp}} = 1/(\rho \, \sigma_{NN})$ ≈ 2 fm, based on an average NN scattering cross section $\sigma_{NN} = 30$ mb [31] at 190 MeV and the nuclear saturation density $\rho = 0.16$ fm^{-3}. Therefore, nuclear bremsstrahlung can be quenched for a photon wavelength $\lambda \geq \lambda_{\mathrm{mfp}}$ or a photon energy $E_\gamma \leq \hbar c/\lambda_{\mathrm{mfp}} \approx 90$ MeV. The strength of quenching of course increases with decreasing photon energy. In a simplified model based

on the classical description of bremsstrahlung production in hard collisions we have estimated the analytical shape of the LPM effect in a two-step p+nucleus reaction [14]. Each segment of the proton trajectories defines a production amplitude with a definite relative phase and therefore must be added coherently. The time between two collisions is characterized by the mean collision time $\tau = \lambda_{\mathrm{mfp}}/(g\beta_0 c) = \tau_0/g$ with β_0 the incoming proton velocity, *i.e.* $\tau_0 \approx 4$ fm/c. The factor g takes into account that in subsequent collisions the velocity of the leading particle is reduced. A value $g \approx 0.5$ is expected to describe the mean time between the first and second collision, *i.e.*, $\tau \approx 8$ fm/c. Averaging over the time distribution $(1/\tau)\exp{(-t/\tau)}$ we derive the following quenching factor, whose analytical form is motivated by several theoretical calculations [7, 11, 32]:

$$f_q = \xi \left(1 - \frac{\alpha}{1 + \left(\frac{E_\gamma}{\hbar}\tau\right)^2} \right).$$ (1)

The parameter α is related to the fraction of energy remaining for the leading particle in subsequent collisions [14], *i.e.*, $\alpha \approx 1/g^2 \approx 0.25$. ξ is an overall scaling factor. The INC calculation was adjusted in an ad hoc manner to account for medium effects by multiplying the spectrum obtained from INC with the quenching factor f_q from Eq. (1).

The experimental data were fitted with the product (INC$\cdot f_q$), where INC represents the full INC spectrum and α, ξ and τ are free parameters. For the spectra obtained at three different angles of $75°$, $115°$ and $155°$ we find $\alpha \approx 1$ and a mean collision time $\tau = 2.4 \pm 0.6$ fm/c for the Ni, Ag and Au targets and 3.7 ± 0.5 fm/c for the C target. These values for the collision time are much smaller than the expected average time interval between two hard NN collisions in nuclei (8 fm/c, see above). From this observation one must conclude that hard NN collisions alone are insufficient to explain the quenching of soft photons. Other effects likely to increase the observed collision frequency (reduced parameter τ) may be multiple soft collisions, but also a modification of the elementary photon production process in the nuclear medium. The latter hypothesis is supported by the observation that the dipole contribution expected from the elementary proton–neutron angular distribution appears to be absent in the reactions studied here (see Fig. 7), as was observed also elsewhere [33]. In our data we observe the corresponding result also from the fact that ξ increases from $\xi = 0.96 \pm 0.06$ at $75°$ to $\xi = 4.3 \pm 2.0$ at $155°$.
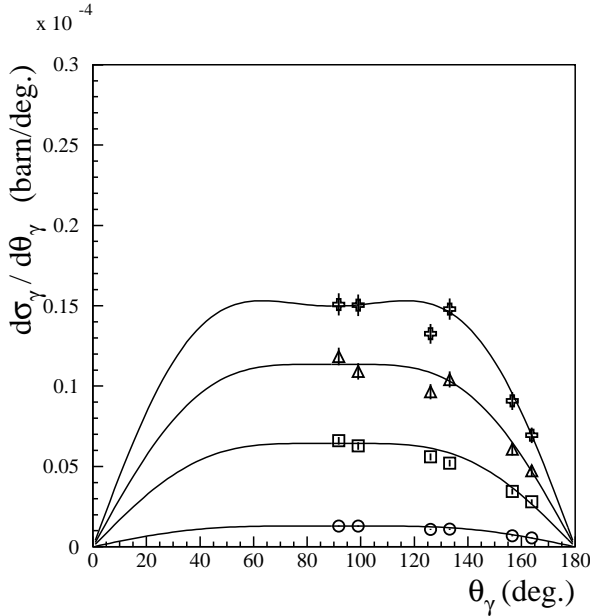
Fig. 7. Photon angular distribution in the NN center-of-mass system for photon energies above 40 MeV for 190 MeV $p+$C. The lines are the result of fits using an isotropic and a dipole component.

6. Soft photons in quantum transport theory

The separation between dynamical effects and LPM quenching is complicated due to the partitioning of the NN interaction in the nuclear medium into a mean-field and a collision component in the models. The available dynamical models are all of semiclassical nature and our new data indicate the need to include consistently the medium modifications and the interference phenomena. The development of a quantum transport theory for photon production in intermediate-energy proton+nucleus reactions, was already started in Ref. [34] but did not go beyond the conventional quasi-particle approximation, *i.e.*, the correlations and off-shell nucleon propagation in the medium were not taken into account. A new approach has been taken up recently [9]. The in-medium photon production cross section is calculated from a microscopic NN interaction including the spectral width of the baryon propagators. Two sources of multiple-scattering effects can be identified: one of minor importance is scattering of final state nucleons before or after photon radiation; more significant appears to be the multiple scattering during off-shell nucleon propagation before the photon is emitted. Preliminary results [35] for a 200 MeV $p+$nucleus reaction indicate that this

approach leads to a remarkable suppression of soft photons below 80 MeV, in qualitative agreement with our data. This approach requires, however, a non-zero temperature of the target nucleons. Recently, another theoretical approach [36] was taken where the kinetic equations that determine the evolution of the two-particle Green's function in matter were derived in the transport approximation for soft-photon production. The correlations in the medium allow multiple scattering to occur without requiring multiple hard collisions, thus yielding Eq. (1) with $f_q(\alpha = 1, \tau = \tau_0)$, *i.e.* $g = 1$, in agreement with the empirical result. We thus obtain an energy dependence of the photon spectrum with the functional form

$$f_E \sim \frac{E_\gamma}{E_\gamma^2 + \left(\frac{\hbar}{\tau_0}\right)^2 \left(\frac{Z}{N}\right)^2} \, \beta_0^2 \, \left(1 - \frac{E_\gamma}{E_{\max}}\right). \qquad (2)$$

This spectrum incorporates the factor $1 - E_\gamma/E_{\max}$ to describe the kinematic limit which is absent in the soft photon approach. (The precise form of this limit may vary, *cf.* [33].) The proton to neutron ratio (Z/N) describes the reduced quenching observed in heavy nuclei. The absolute cross section is determined by the geometrical reaction cross section.
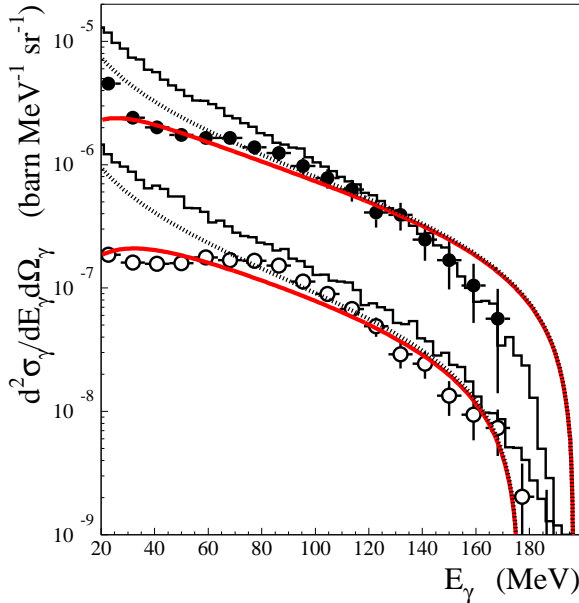

Fig. 8. Photon spectrum at a laboratory angle of $75°$ for 190 MeV $p+$Au (top, filled circles) and $p+$C (bottom, circles). The histograms indicate the results from the INC model. The solid curves are obtained using Eq. (2), the dotted grey lines correspond to Eq. (2) with the collision frequency set to zero.

The suppression of soft photons can be described quantitatively as shown in Fig. 8 by the solid lines. The amount of quenching can be seen from a comparison with the result where the collision frequency (*i.e.*, $\hbar/\tau_0$) is set to zero (the dotted curves). This approaches the quasi-free result of the INC model. Eq. (2) describes also well the published data [23, 33, 37] for 168 MeV p+Tb and 145 MeV p+Pb by only adjusting β_0 according to the respective beam energy, see Fig. 9. This shows that also at lower beam energy quenching occurs, but the effect at photon energies above 30 MeV is small and went unnoticed so far.
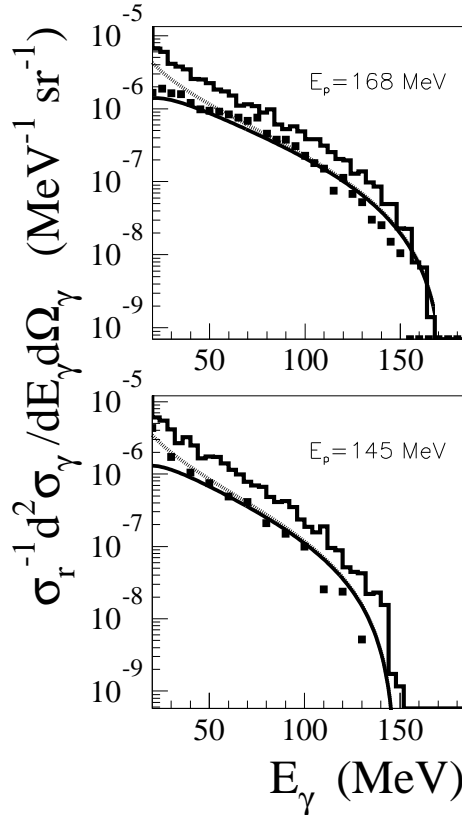
Fig. 9. Photon spectrum at a laboratory angle of 90° for 168 MeV p+Tb (top, filled squares) and 145 MeV p+Pb (bottom, filled squares). The histograms indicate the results from the INC model. The solid curves are obtained using Eq. (2), the dotted curves correspond to Eq. (2) with the collision frequency set to zero.

In summary, we observe a strong suppression of the soft bremsstrahlung cross section in comparison with the prediction of transport models that include bremsstrahlung on basis of quasi-free nucleon–nucleon collisions. New

theoretical models are being developed using simplified reaction dynamics but taking into account medium effects such as nucleon correlations and off-shell propagation of the nucleons involved in the photon production. An analytical form for the bremsstrahlung production in nuclear matter based on these assumptions was obtained which describes the suppression of soft bremsstrahlung. These results show the importance of multiple-scattering processes beyond the classical picture of multiple hard collisions.

7. Outlook to pionic fusion

A highly coherent mechanism is required if the production of a single pion in a nuclear reaction demands a significant fraction of the available energy. In the extreme limit, the total excess energy may be concentrated in the pion field, the pion is emitted and the colliding nuclei fuse to a united nucleus in a specific bound state.

In nuclear reactions mesons can be produced at collision energies per nucleon which are considerably below the threshold energy in the free nucleon–nucleon system. Dynamical phase-space calculations provide a reasonable prediction at energies close to the meson production threshold. They underestimate, however, severely the cross sections at energies deeply below the threshold, *i.e.* for a threshold fraction $f < 0.2$ [38], where f is the kinetic energy per nucleon above the Coulomb barrier, divided by the threshold kinetic energy E_{thr}^{NN}. Quantal and dynamical fluctuations have been studied but the calculations still underestimate the data [39]. This unsatisfactory situation reflects the current poor understanding of the relevant many-body processes and raises the question, which mechanisms govern the transfer of energy to the meson channel. The required high relative energy among colliding nucleons might originate from many-body correlations or cooperative multiple collisions. Also multi-step processes with intermediate nucleon resonances might act as "energy storage" to concentrate the required meson-production energy.

In order to gain insight into this genuine quantum many-body problem and to provide clear test cases for theory, well-defined and simple reactions need to be addressed. This will gain the necessary restrictions on relevant quantum numbers (spin, isospin) and provide the selectivity for particular processes. Sub-nucleonic degrees of freedom in nuclei are involved through the intermediate excitation of nucleon resonances. In contrast with inclusive pion production, where the phase-space of the unobserved system dominates the cross section, we consider the extreme limit of pionic fusion, *i.e.* the exclusive two-body reaction $A_1 + A_2 \rightarrow B(J, I) + \pi$ leading to a specific bound state of the final nucleus B with spin and isospin quantum numbers J and I, respectively. The center-of-mass kinetic energy $T_{\text{c.m.}}^{\text{in}}$ in the incident channel is transferred to the two-body exit channel including the pion field:

$$T_{\text{c.m.}}^{\text{in}} = T_{\text{c.m.}}^{\text{ex}} + Q_{A_1 A_2, B} + m_\pi c^2 \,,$$

where Q denotes the Q-value of the complete fusion process. In this case there are no "spectator" nucleons and the reaction is highly coherent. The cross section is determined by the properties of the transition amplitude which contains the details on the reaction dynamics and the structure of the nuclear fragments.

It is the experimental challenge to explore suitable target-projectile combinations in order to limit the number of possible intermediate states. Starting with an isoscalar entrance channel, the nature of the pion-production process necessitates a spin and isospin change by one unit, thus leaving the final nucleus in an isospin $I = 1$ state. The complete microscopic calculation of such a process is a theoretical challenge which involves a correct description of the nuclear wave functions, the elementary pion-nucleon interaction and the de-excitation of the final pion-nucleus system. The sensitivity to properties of intermediate baryonic resonances makes the pionic fusion process an important and decisive tool.

A scarce body of data is available for pionic fusion in light systems as $p + p$, $p + d$ and ^{3}He+^{3}He. Truly microscopic calculations are limited to cases where the projectile is a proton [40]. The cross sections are qualitatively described, but severely underestimated, in a microscopic reaction model including intermediate baryon resonance excitation [41]. In a novel experimental approach (see setup in Fig. 10) we intend to study the pionic fusion process by exclusive pion production in overdetermined kinematics.
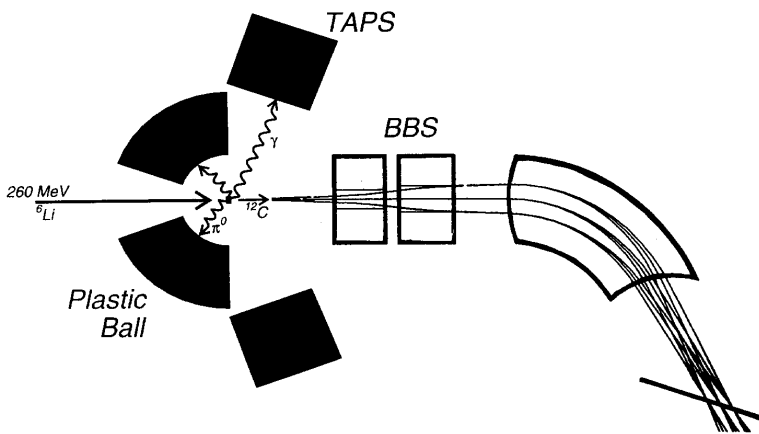

Fig. 10. The proposed experimental setup for ^{6}Li+^{6}Li pionic fusion studies using the BBS spectrometer, the TAPS photon spectrometer and the Plastic Ball backward hemisphere for neutral pions.

This requires a suitable combination of detector systems that allow to measure the emitted pion, the residual nucleus and the γ decay from the fused system in order to determine the excited state. Only in this way one can guarantee cleaner and truly exclusive data providing also the angular distribution of pions. In particular, we aim to study here the reaction

$$^{6}\mathrm{Li}\,(I=0) +^{6}\mathrm{Li}\,(I=0) \rightarrow^{12}\mathrm{C}^{*}(I=1) + \pi^{0}$$
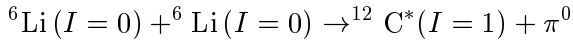
leading to the 15.1 MeV excited state of ^{12}C which can be detected by the M1 γ decay to the ground state. A beam energy of 260 MeV will lead to about 7 MeV above the absolute threshold for the 15.1 MeV excited state. This choice will produce pion momenta $k_{\pi} \approx 40$ MeV/c and allows a comparison with the ^{12}C+^{12}C data from Ref. [42]. Our reaction offers ideal conditions for the detection of all final-state particles.

8. Conclusions

In heavy-ion reactions an additional source of photon emission, softer than the one originating in the well-known first-chance $pn\gamma$ process, has been observed, accounting for up to a third of the total bremsstrahlung yield. The origin of this second component has been localised in secondary $NN\gamma$ collisions within a thermalizing system.

The investigation of coherent bremsstrahlung production in the reaction $p(\alpha, \gamma)$ at $50A$ MeV has demonstrated that the high-energy photon spectrum is dominated by capture to form ^{5}Li. Such results have motivated the extension of this technique to study radiative capture of protons on the halo nucleus ^{6}He. In addition to the $p(^{6}\mathrm{He}, \gamma)\,^{7}$Li reaction, evidence for quasi-free capture on subsystems (^{5}He, α and n) of ^{6}He has been found. Of particular importance is the observation of events which correspond to the previously measured $p(\alpha, \gamma)$ reaction, as well as the non-observation of capture on a di-neutron.

New experimental data have been presented for nuclear bremsstrahlung from the soft-photon region up to the kinematic limit in proton+nucleus reactions. A strong suppression of the soft bremsstrahlung cross section is observed contrary to expectations based on quasi-free NN collisions. In order to explain this result, medium effects such as nucleon correlations and off-shell propagation of the nucleons involved in the photon production need to be considered in collisions where the mean-free path is shorter than the coherence length of the produced photons.

In a future experiment the highly coherent mechanism of pionic fusion will be studied in an exclusive experiment.

The effort of the AGOR team in providing high-quality beam is gratefully acknowledged. We thank L. Dieperink, A. Korchin, O. Scholten and A. Sedrakian for valuable discussions and providing results from their calculations. This work was supported in part by FOM, the Netherlands, by IN2P3 and CEA, France, BMBF and DFG, Germany, DGICYT and the Generalitat Valencia, Spain, by GACR, Czech Republic, and by the European Union HCM network contract HRXCT94066.

REFERENCES

[1] H. Nifenecker, *Prog. Part. Nucl. Phys.* **23**, 271 (1989).

[2] Y. Schutz, *et al.*, *Nucl. Phys.* **A622**, 405 (1997).

[3] G. Martínez *et al.*, *Phys. Lett.* **B334**, 23 (1994).

[4] L.D. Landau, I. Pomerančuk, *Dokl. Akad. Nauk SSSR* **92**, 553 (1953); A.B. Migdal, *Sov. Phys. JETP* **5**, 527 (1957).

[5] J. Benisz, Z. Chylinski, W. Wolter, *Nuovo Cim. XI* **4**, 525 (1959).

[6] S. Klein, *Rev. Mod. Phys.* **71**, 1501 (1999).

[7] J. Knoll, D.N. Voskresensky, *Phys. Lett.* **B351**, 43 (1995); *Ann. Phys.* **249**, 532 (1996).

[8] A.V. Koshelkin, *Phys. Rev.* **C59**, 936 (1999).

[9] A. Sedrakian, A.E.L. Dieperink, *Phys. Lett.* **B463**, 145 (1999), and private communication.

[10] E.V. Shuryak, *Phys. Lett.* **B231**, 175 (1989).

[11] J. Cleymans, V.V. Goloviznin, K. Redlich, *Phys. Rev.* **D47**, 173 (1993).

[12] H. Ströher, *Nuclear Physics News* **6**, 7 (1996).

[13] A.R. Gabler *et al.*, *Nucl. Instrum. Methods Phys. Res., Sect.* **A346**, 168 (1994).

[14] M.J. van Goethem, PhD thesis, Univ. Groningen 2000.

[15] L. Aphecetche *et al.*, *Phys. Lett.* **B519**, 8 (2001).

[16] D. Stracener *et al.*, *Nucl. Instrum. Methods Phys. Res., Sect.* **A294**, 485 (1990).

[17] H. Leegte *et al.*, *Nucl. Instrum. Methods Phys. Res., Sect.* **A313**, 26 (1992).

[18] D.G. d'Enterria *et al.*, *Phys. Rev. Lett.* **87**, 022701 (2001).

[19] M. Hoefman *et al.*, *Phys. Rev. Lett.* **85**, 1404 (2000).

[20] E. Sauvan *et al.*, *Phys. Rev. Lett.* **87**, 042501 (2001).

[21] F.M. Marqués *et al.*, *Phys. Lett.* **B476**, 219 (2000).

[22] M.J. van Goethem *et al.*, `nucl-ex0111021`, submitted to *Phys. Rev. Lett.*

[23] M. Kwato Njock *et al.*, *Phys. Lett.* **B207**, 269 (1988).

[24] Y. Schutz *et al.*, *Nucl. Phys.* **A622**, 404 (1997).

[25] G. Martínez *et al.*, *Phys. Lett.* **B461**, 28 (1999).

[26] J. Cugnon, *Nucl. Phys.* **A489**, 781 (1988).

[27] J. Cugnon *et al.*, *Nucl. Phys.* **A620**, 475 (1997).

[28] M.J. van Goethem *et al.*, to be published.

[29] A.Yu. Korchin, O. Scholten, *Phys. Rev.* **C58**, 1098 (1998).

[30] W. Cassing *et al.* *Phys. Rep.* **188**, 363 (1990).

[31] J. Franz *et al.*, *Nucl. Phys.* **A490**, 667 (1988).

[32] T. Alm *et al.*, *Phys. Rev.* **C52**, 1972 (1995).

[33] J. Clayton *et al.*, *Phys. Rev.* **C45**, 1815 (1992).

[34] K. Nakayama, G.F. Bertsch, *Phys. Rev.* **C40**, 2520 (1989).

[35] A. Sedrakian, private communication.

[36] A.V. Koshelkin, private communication.

[37] J.A. Pinston *et al.*, *Phys. Lett.* **B218**, 128 (1989).

[38] G. Martínez *et al.*, *Phys. Rev. Lett.* **83**, 1538 (1999).

[39] M. Belkacem, E. Suraud, S. Ayik, *Phys. Rev.* **C47**, R16 (1993).

[40] H.W. Fearing, *Prog. Part. Nucl. Phys.* **7**, 113 (1981).

[41] L. Harzheim, M.G. Huber, B.C. Metsch, *Z. Phys.* **A340**, 399 (1991).

[42] D. Horn *et al.*, *Phys. Rev. Lett.* **77**, 2408 (1996).